



Heavy atom enhanced generation of singlet oxygen in novel indenofluorene-based two-photon absorbing chromophores for photodynamic therapy



Changquan Tang¹, Ping Hu¹, En Ma¹, Mingdong Huang¹, Qingdong Zheng^{*}

State Key Laboratory of Structural Chemistry, Fujian Institute of Research on the Structure of Matter, Chinese Academy of Sciences, 155 Yangqiao West Road, Fuzhou 350002, PR China

ARTICLE INFO

Article history:

Received 2 December 2014
Received in revised form
17 January 2015
Accepted 20 January 2015
Available online 3 February 2015

Keywords:

Two-photon absorption
Photodynamic therapy
Singlet oxygen
Heavy atom effect
Cytotoxicity
Photosensitizer

ABSTRACT

A series of indenofluorene-based two-photon absorbing chromophores (**FL0**, **FL-2BrN**, **FL-1IN**, **FL-2IN**, and **FL-2IS**) have been designed and synthesized for photodynamic therapy (PDT). Two-photon absorption (TPA) properties of these chromophores are determined and their structure-property relationship has been established. By incorporating electron withdrawing halogen atoms (such as Br, I) into the π -conjugation backbone of the chromophores, enhanced TPA cross-section values up to 2707 GM were achieved due to the formation of a donor-acceptor-donor (D-A-D) motif. At the same time, upon excitation at 430 nm, 2.2–4.1 times of enhancement in the singlet oxygen generation yield was observed for the photosensitizers with the heavy atoms incorporated. The photosensitizers with heavy atoms also show increased singlet oxygen generation efficiencies upon two-photon excitation at 808 nm, compared to those photosensitizers without heavy atoms. Photocytotoxicity of **FL-2IN** against cancer cells via two-photon excitation (808 nm) demonstrated that the indenofluorene-based chromophores are effective singlet oxygen donors for two-photon PDT.

© 2015 Elsevier Ltd. All rights reserved.

1. Introduction

In the past two decades, photodynamic therapy (PDT) has been established as a valid clinical treatment method for cancer and other diseases [1–3]. In PDT, a photosensitizer is excited to its singlet excited state by the absorption of a photon, and decays to its triplet excited state via intersystem crossing (ISC). The photosensitizer in the triplet state can subsequently transfer its energy to the surrounding oxygen in the ground state ($^3\text{O}_2$), resulting in generation of singlet oxygen ($^1\text{O}_2$) [4,5]. Singlet oxygen is a highly reactive oxygen species that can damage biological cell components such as lipids [6], nucleic acids [7,8], or proteins [9,10]. In current PDT, one of the main problems is the limited penetration of visible light into tissue, restricting PDT to the treatment of ailments on tissue surface [11].

Two-photon absorption (TPA) is a nonlinear process where a molecule is promoted to its excited states by absorbing two low-

frequency (long-wavelength) photons. With two-photon excitation, near IR light at 750–1000 nm where tissue is more transparent can be used to activate the photosensitizers for $^1\text{O}_2$ generation [12]. Besides a deep tissue penetration, another advantage of two-photon PDT is that the treatment is localized at the focal point of a laser beam because the TPA process quadratically depends on the laser intensity, which provides a more precise treatment [13]. The key prerequisite for two-photon PDT is that the photosensitizers should efficiently generate $^1\text{O}_2$ under two-photon excitation. To obtain more efficient two-photon photosensitizers, much effort have been devoted to improve TPA cross-sections of traditional photosensitizers (such as porphyrins) via conjugating peripheral energy donors with large TPA cross sections [14–16], or to synthesize new photosensitizers with large TPA cross sections [17–20].

A molecule with large TPA generally should have an extended π -conjugation system with good planarity, and strong electron acceptors and (or) donors attached in the terminals because the TPA cross section value for a given molecule is related to the extent of intramolecular charge transfer of the molecule upon photoexcitation. Ladder-type oligo-*p*-phenylenes are good building blocks to construct materials with large TPA cross-section values owing to

* Corresponding author. Tel./fax: +86 591 83721625.

E-mail address: qingdongzheng@fjirsm.ac.cn (Q. Zheng).

¹ Tel./fax: +86 591 83721625.

their planar chemical structures with extended π -conjugation [21,22]. In our previous reports, the relationship between TPA properties of ladder-type oligo-*p*-phenylene-cored chromophores and their conjugation lengths was systematically investigated [23,24]. It was found that the TPA cross section values of the ladder-type oligo-*p*-phenylenes-cored chromophores increase with the increasing π -conjugation lengths of the central ladder-type oligo-*p*-phenylene core. On the other hand, it has been found that promoting an ISC rate is an efficient method to improve the singlet oxygen generation of a chromophore. The rate of ISC can be enhanced by strong spin-orbit coupling in the presence of heavy atoms (such as I, Br) which are incorporated into the chromophore or are external but close enough to the chromophore, termed as a heavy atom effect [25–27]. On the basis of these considerations, we design a series of indenofluorene-based chromophores with heavy halogen atoms incorporated and anticipate that the introduction of heavy halogen atoms into the chromophores will lead to promising photosensitizers with large TPA cross sections and high $^1\text{O}_2$ generation rates. Although the two-photon properties of indenofluorene-based chromophores have been investigated [28–30], their $^1\text{O}_2$ generation properties under two-photon excitation are still unexplored. Hence, the heavy atom effect on the TPA as well as $^1\text{O}_2$ generation has never been reported to the best of our knowledge.

In this paper, we report on the design and synthesis of a series of novel indenofluorene-based chromophores as two-photon PDT photosensitizers by incorporating heavy halogen atoms (Chart 1). The linear and TPA properties, as well as the one- and two-photon excited fluorescence properties for these chromophores were investigated. Singlet oxygen generation efficiencies for these photosensitizers under one- and two-photon excitation have also been evaluated. The application of chromophore **FL-2IN** as a photosensitizer for two-photon photodynamic therapy was successfully demonstrated.

2. Experimental section

2.1. Materials and instruments

Reagents were purchased from Aldrich Inc. and Adamas-beta Chemical Ltd. and used without further purification unless otherwise stated. The starting materials **1** [23], **3** [31], **4** [31], **6** [32], **7**

[33,34], and **8** [35,36] were prepared according to the literature procedures. Column chromatography was conducted with silica gel 60 (200–300 mesh). ^1H NMR and ^{13}C NMR spectra were recorded at 400 and 100 MHz, respectively. The MALDI-TOF spectra were recorded on a Voyager-DE STR mass spectrometer. Absorption and fluorescence spectra were acquired using a spectrometer (Lambda 35 UV/vis) and a Cary fluorimeter, respectively. For nonlinear optical experiments, the excitation pulse (1 KHz, 240–2600 nm, pulse-width <120 fs) was generated from an optical parametric amplifier (TOPAS-F-UV2, Spectra-Physics) pumped by a regeneratively amplified femtosecond Ti-sapphire laser system (800 nm, 1 KHz, pulse energy 4 mJ, pulse-width <120 fs, Spitfire Pro-F1KXP, Spectra-Physics), which is seeded by femtosecond Ti-sapphire oscillator (80 MHz, pulse-width <70 fs, 710–920 nm, Maitai XF-1, Spectra-Physics). The one-photon excitation singlet oxygen emission was measured by using a FLS980 spectrofluorometer. The pump source for two-photon excitation as well as TPA cross-section measurements was generated by a mode locked Ti:sapphire laser. The laser beam was focused by an $f = 10$ cm lens, and the solution sample in a 1 cm fluorimeter cuvette (four optically clear windows) was placed at a fixed distance of ~ 11.5 cm from the focusing lens. Long-pass filter was used to attenuate the excitation laser beam.

2.2. Methods

2.2.1. Cytotoxicity assays

The MCF-7 cells (human breast carcinoma) were cultured in Dulbecco's modified Eagle's medium (DMEM) supplemented with 10% FBS (fetal bovine serum) in an atmosphere of 5% CO_2 and 95% air at 37 °C. Immediately before the experiments, the cells (8000 per well) were placed in a 96-multiwell plate, followed by addition of increasing concentrations of compound **FL-2IN** (99% DMEM and 1% DMSO). The photosensitizer solutions were prepared by dispersing the DMSO solution of **FL-2IN** to the DMEM solution directly to form nanoparticles. The final concentrations of the photosensitizer were 0–40 μM ($n = 4$). The cells were then incubated at 37 °C in an atmosphere of 5% CO_2 and 95% air at 37 °C for 24 h, followed by MTT assays.

2.2.2. Two-photon PDT against cancer cells

MCF-7 cancer cells were placed in 96-multiwell plates about 8000 per well and incubated overnight at 37 °C in a humidified

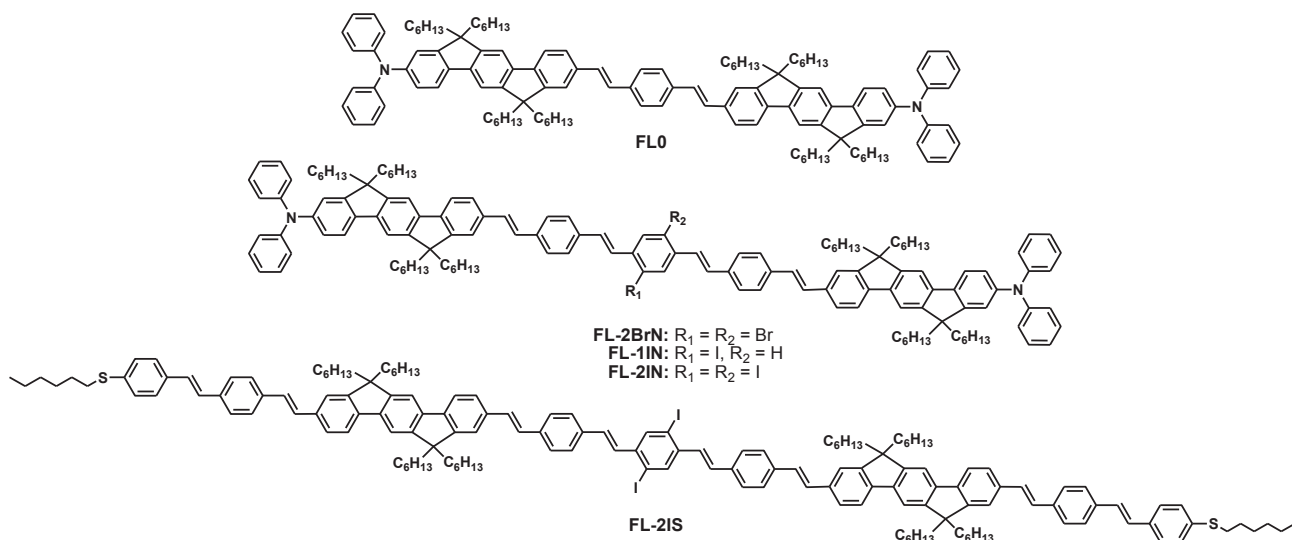


Chart 1. Molecular structures of indenofluorene-based chromophores **FL0**, **FL-2BrN**, **FL-1IN**, **FL-2IN**, and **FL-2IS**.

incubator with 5% CO₂ atmosphere. The DMEM medium was removed, and the cells were treated with the medium (200 μL) containing **FL-2IN** at various concentrations. After incubation 8 h, cells were washed using sterile PBS and added fresh medium. Each well was exposed to laser irradiation at 808 nm with power density of ~3.0 W cm⁻². Then the cells were further incubated for 12 h followed by the MTT colorimetric assay. Cell experiments without photosensitizer under the same experimental conditions were performed as controls.

2.3. Synthesis

2.3.1. Synthesis of compound **2**

A mixture of compound **1** (1.0 g, 1.34 mmol), diphenylamine (0.23 g, 1.34 mmol), and sodium *t*-butoxide (0.15 g, 1.56 mmol) in dry toluene (40 ml) was stirred at room temperature for 30 min under nitrogen atmosphere. Then tri(dibenzylideneacetone)dipalladium(0) (18 mg, 0.027 mmol) and 1,1'-bis(diphenylphosphino)ferrocene (36 mg, 0.054 mmol) were added to the mixture. The mixture was heated to reflux for 12 h and then cooled to room temperature, diluted with diethyl ether (60 ml), and washed with brine and water in sequence. The resulting organic layer was dried over sodium sulfate and concentrated *in vacuo* to give the crude product, and it was purified by column chromatography (eluent: ethyl acetate/petroleum ether = 1/40) on silica gel to afford the title compound as a yellow oil (0.50 g, 45%). ¹H NMR (400 MHz, CDCl₃, 25 °C, TMS): δ = 7.61 (d, *J* = 8.4 Hz, 1H), 7.57 (d, *J* = 8.4 Hz, 1H), 7.51 (d, *J* = 7.6 Hz, 2H), 7.44 (d, *J* = 7.2 Hz, 2H), 7.23 (d, *J* = 7.2 Hz, 4H), 7.11 (d, *J* = 7.6 Hz, 5H), 7.07–6.97 (m, 3H), 2.02–1.84 (m, 8H), 1.18–0.95 (m, 24H), 0.79–0.55 (m, 20H); MS (MALDI-TOF, *m/z*): calcd for C₅₆H₇₀BrN, [M⁺] 835.4; found, 835.5.

2.3.2. Synthesis of compound **5**

Compound **2** (0.5 g, 0.6 mmol), compound **4** (0.1 g, 0.76 mmol), Pd(OAc)₂ (12 mg, 0.05 mmol), P(*o*-tolyl)₃ (61 mg, 0.2 mmol), Et₃N (1.0 ml), CH₃CN (20 ml) were added to a pressure tube with a plunger valve and a magnetic bar under argon. The resulting mixture was heated to reflux for 24 h and then cooled to room temperature. The mixture was poured into methanol (50 ml) with vigorous stirring. The precipitate formed was collected on a filter funnel and washed thoroughly with methanol, and the crude product was purified by column chromatography (eluent: ethyl acetate/petroleum ether = 1/15) on silica gel to afford the title compound as a yellow solid. The title compound was obtained as a yellow crystalline solid (0.26 g, 49%). ¹H NMR (400 MHz, CDCl₃, 25 °C, TMS): δ = 10.00 (s, 1H), 7.89–7.84 (m, 2H), 7.76–7.68 (m, 3H), 7.61 (d, *J* = 7.6 Hz, 1H), 7.58–7.51 (m, 5H), 7.39 (d, *J* = 8.4 Hz, 1H), 7.23 (d, *J* = 7.6 Hz, 4H), 7.12 (d, *J* = 7.6 Hz, 5H), 7.17–6.98 (m, 3H), 2.08–1.86 (m, 8H), 1.17–0.95 (m, 24H), 0.81–0.54 (m, 20H); MS (MALDI-TOF, *m/z*): calcd for C₆₅H₇₇NO, [M⁺] 887.6; found, 887.6.

2.3.3. Synthesis of compound **9**

This compound was prepared using a similar procedure to that used for the synthesis of **5**. Quantities: compound **1** (0.748 g, 1.0 mmol), (*E*)-hexyl(4-(4-vinylstyryl)phenyl)sulfane (0.28 g, 0.87 mmol), Pd(OAc)₂ (12 mg, 0.05 mmol), P(*o*-tolyl)₃ (61 mg, 0.2 mmol), Et₃N (1.0 ml), CH₃CN (20 ml). The title compound was obtained as a yellow solid (0.56 g, 57%). ¹H NMR (400 MHz, CDCl₃, 25 °C, TMS): δ = 7.71 (d, *J* = 8.4 Hz, 1H), 7.68–7.56 (m, 4H), 7.55–7.46 (m, 4H), 7.45–7.37 (m, 5H), 7.30 (d, *J* = 8.4 Hz, 2H), 7.22–7.13 (m, 2H), 7.08 (s, 2H), 2.94 (t, *J* = 7.6 Hz, 2H), 2.10–1.92 (m, 8H), 1.71–1.63 (m, 2H), 1.51–1.37 (m, 4H), 1.35–1.21 (m, 5H), 1.12–0.83 (m, 24H), 0.81–0.56 (m, 20H); MS (MALDI-TOF, *m/z*): calcd for C₆₆H₈₅BrS, [M⁺] 988.5; found, 988.6.

2.3.4. Synthesis of compound **10**

This compound was prepared using a similar procedure to that used for the synthesis of **5**. Quantities: compound **9** (0.60 g, 0.61 mmol), compound **4** (0.16 g, 1.21 mmol), Pd(OAc)₂ (12 mg, 0.05 mmol), P(*o*-tolyl)₃ (61 mg, 0.2 mmol), Et₃N (1.0 ml), CH₃CN (20 ml). The title compound was obtained as a yellow crystalline solid (0.33 g, 52%). ¹H NMR (400 MHz, CDCl₃, 25 °C, TMS): δ = 10.00 (s, 1H), 7.89 (d, *J* = 8.4 Hz, 2H), 7.77–7.66 (m, 4H), 7.61–7.47 (m, 10H), 7.45–7.36 (m, 2H), 7.30 (d, *J* = 8.4 Hz, 3H), 7.22–7.16 (m, 3H), 7.09 (s, 2H), 2.94 (t, *J* = 7.6 Hz, 2H), 2.12–1.96 (m, 8H), 1.73–1.66 (m, 2H), 1.48–1.40 (m, 2H), 1.37–1.23 (m, 7H), 1.17–0.96 (m, 24H), 0.91–0.63 (m, 20H); MS (MALDI-TOF, *m/z*): calcd for C₇₅H₉₂OS, [M⁺] 1040.6; found, 1040.7.

2.3.5. Synthesis of compound **FLO**

This compound was prepared using a similar procedure to that used for the synthesis of **5**. Quantities: compound **2** (0.80 g, 0.96 mmol), compound **3** (50 mg, 0.38 mmol), Pd(OAc)₂ (12 mg, 0.05 mmol), P(*o*-tolyl)₃ (61 mg, 0.2 mmol), Et₃N (1.0 ml), CH₃CN (20 ml). The title compound was obtained as a yellow crystalline solid (0.29 g, 46%). ¹H NMR (400 MHz, CDCl₃, 25 °C, TMS): δ = 7.70 (d, *J* = 7.6 Hz, 2H), 7.63 (d, *J* = 8.0 Hz, 2H), 7.60–7.48 (m, 12H), 7.29–7.17 (m, 12H), 7.12 (d, *J* = 7.6 Hz, 10H), 7.06 (d, *J* = 8.0 Hz, 2H), 7.02–6.98 (m, 4H), 2.10–1.82 (m, 16H), 1.12–0.83 (m, 48H), 0.81–0.56 (m, 40H); ¹³C NMR (100 MHz, CDCl₃, 25 °C, TMS): δ = 152.65, 151.64, 150.52, 150.12, 148.08, 146.87, 141.55, 140.46, 139.71, 136.90, 136.83, 135.83, 129.34, 129.17, 127.23, 126.81, 125.67, 123.90, 123.65, 122.38, 120.68, 120.13, 119.83, 119.54, 113.84, 113.40, 54.78, 54.72, 40.90, 40.58, 31.62, 31.59, 29.82, 29.68, 23.81, 22.62, 22.56, 14.07. MS (MALDI-TOF, *m/z*): calcd for C₁₁₁H₁₄₇S₂, [M⁺] 1641.1; found, 1641.9. Elemental analysis: calcd for C₁₁₁H₁₄₇S₂: C 89.21, H 9.08, N 1.71; found: C 89.52, H 8.93, N 1.95.

2.3.6. Synthesis of compound **FL-2BrN**

To compound **6** (68 mg, 0.126 mmol) in dry THF (30 ml), was added sodium *tert*-butoxide (0.146 g, 1.52 mmol). The reaction mixture was cooled to 0 °C in an ice bath. Compound **5** (0.26 g, 0.29 mmol) was added to the solution, the ice bath was removed and the mixture was stirred at room temperature for 12 h. The reaction mixture was poured into 100 ml of water and then THF was removed. The crude product was collected by filtration and further purified by column chromatography with ethyl acetate/petroleum ether (1/40), affording the title compound as a yellow crystalline solid (0.19 g, 77%). ¹H NMR (400 MHz, CDCl₃, 25 °C, TMS): δ = 7.91 (s, 2H), 7.71 (d, *J* = 8.0 Hz, 2H), 7.63 (d, *J* = 8.0 Hz, 2H), 7.61–7.56 (m, 14H), 7.52 (d, *J* = 18.4 Hz, 2H), 7.41 (d, *J* = 15.6 Hz, 2H), 7.35–7.18 (m, 12H), 7.17–7.10 (m, 12H), 7.07–7.06 (m, 2H), 7.05–6.98 (m, 4H), 2.12–1.85 (m, 16H), 1.20–0.96 (m, 48H), 0.88–0.56 (m, 40H); ¹³C NMR (100 MHz, CDCl₃, 25 °C, TMS): δ = 152.63, 151.66, 150.52, 150.11, 148.05, 146.87, 141.72, 140.50, 139.63, 137.92, 136.85, 135.70, 135.61, 131.88, 130.32, 129.99, 129.16, 127.44, 126.95, 126.84, 125.77, 125.40, 123.87, 123.64, 123.13, 122.37, 120.73, 120.13, 119.80, 119.55, 113.86, 113.38, 54.76, 54.72, 40.87, 40.55, 31.60, 31.57, 29.80, 29.65, 23.79, 22.60, 22.54, 14.06, 14.04. MS (MALDI-TOF, *m/z*): calcd for C₁₃₈H₁₅₈Br₂N₂, [M⁺] 2004.5; found, 2004.1. Elemental analysis: calcd for C₁₃₈H₁₅₈Br₂N₂: C 82.69, H 7.94, N 1.40; found: C 82.75, H 8.01, N 1.26.

2.3.7. Synthesis of compound **FL-11N**

This compound was prepared using a similar procedure to that used for the synthesis of **FL-2BrN**. Quantities: compound **7** (70 mg, 0.14 mmol), sodium *tert*-butoxide (0.16 g, 1.67 mmol), compound **5** (0.30 g, 0.34 mmol), THF (40 ml). The title compound was obtained as a yellow crystalline solid (0.18 g, 64%). ¹H NMR (400 MHz, CDCl₃, 25 °C, TMS): δ = 8.11 (d, *J* = 7.6 Hz, 2H), 7.89 (d, *J* = 8.4 Hz, 2H),

7.77–7.66 (m, 4H), 7.63 (d, $J = 8.4$ Hz, 4H), 7.60–7.45 (m, 12H), 7.43–7.39 (m, 2H), 7.29–7.17 (m, 10H), 7.16–7.11 (m, 10H), 7.09–7.07 (m, 2H), 7.05–6.98 (m, 6H), 2.12–1.82 (m, 16H), 1.18–0.96 (m, 48H), 0.84–0.52 (m, 40H); ^{13}C NMR (100 MHz, CDCl_3 , 25 °C, TMS): $\delta = 152.64, 151.66, 150.53, 150.13, 148.08, 146.88, 141.66, 140.49, 139.66, 139.12, 138.42, 137.65, 137.57, 137.50, 136.88, 136.12, 136.02, 135.70, 131.75, 131.00, 129.77, 129.52, 129.15, 127.27, 127.07, 126.83, 126.41, 126.25, 125.98, 125.74, 123.88, 123.65, 122.37, 120.72, 120.11, 119.83, 119.53, 113.85, 113.39, 54.77, 54.72, 40.85, 40.54, 31.59, 31.56, 29.79, 29.65, 23.80, 22.59, 22.53, 14.03, 14.01$. MS (MALDI-TOF, m/z): calcd for $\text{C}_{138}\text{H}_{159}\text{I}_2\text{N}_2$, $[\text{M}^+]$ 1972.6; found, 1972.2. Elemental analysis: calcd for $\text{C}_{138}\text{H}_{159}\text{I}_2\text{N}_2$: C 84.02, H 8.12, N 1.42; found: C 84.19, H 8.11, N 1.12.

2.3.8. Synthesis of compound FL-2IN

This compound was prepared using a similar procedure to that used for the synthesis of FL-2BrN. Quantities: compound **8** (85 mg, 0.13 mmol), sodium *tert*-butoxide (0.16 g, 1.67 mmol), compound **5** (0.30 g, 0.34 mmol), THF (40 ml). The title compound was obtained as a yellow crystalline solid (0.24 g, 88%). ^1H NMR (400 MHz, CDCl_3 , 25 °C, TMS): $\delta = 8.07$ (s, 1H), 7.70 (d, $J = 8.0$ Hz, 2H), 7.60 (d, $J = 8.0$ Hz, 4H), 7.59–7.48 (m, 16H), 7.38 (d, $J = 17.6$ Hz, 2H), 7.29–7.16 (m, 10H), 7.14–7.10 (m, 12H), 7.05–7.02 (m, 2H), 7.01–6.97 (m, 6H), 2.12–1.84 (m, 16H), 1.19–0.97 (m, 48H), 0.81–0.56 (m, 40H); ^{13}C NMR (100 MHz, CDCl_3 , 25 °C, TMS): $\delta = 152.64, 151.75, 151.66, 150.53, 150.12, 148.06, 146.88, 143.86, 141.72, 140.80, 140.51, 139.64, 137.88, 136.86, 136.71, 136.38, 136.32, 136.13, 135.64, 135.11, 132.01, 131.90, 130.37, 130.32, 130.10, 129.97, 129.17, 127.43, 127.20, 126.98, 126.85, 126.76, 126.71, 125.79, 123.88, 123.69, 123.65, 122.38, 120.73, 120.14, 119.81, 119.56, 113.87, 113.40, 54.77, 54.73, 40.87, 40.56, 31.61, 31.58, 29.81, 29.78, 29.74, 29.66, 23.80, 22.62, 22.55, 14.07, 14.06$. MS (MALDI-TOF, m/z): calcd for $\text{C}_{138}\text{H}_{158}\text{I}_2\text{N}_2$, $[\text{M}^+]$ 2098.5; found, 2098.4. Elemental analysis: calcd for $\text{C}_{138}\text{H}_{158}\text{I}_2\text{N}_2$: C 78.98, H 7.59, N 1.33; found: C 79.24, H 7.69, N 1.04.

2.3.9. Synthesis of compound FL-2IS

This compound was prepared using a similar procedure to that used for the synthesis of FL-2BrN. Quantities: compound **8** (85 mg, 0.13 mmol), sodium *tert*-butoxide (0.16 g, 1.67 mmol), compound **10** (0.33 g, 0.31 mmol), THF (40 ml). The title compound was obtained as a yellow crystalline solid (0.26 g, 83%). ^1H NMR (400 MHz, CDCl_3 , 25 °C, TMS): $\delta = 8.12$ (s, 2H), 7.79–7.72 (m, 4H), 7.69–7.58 (m, 12H), 7.57–7.49 (m, 10H), 7.45–7.40 (m, 6H), 7.39–7.29 (m, 10H), 7.25–7.16 (m, 5H), 7.09 (d, $J = 5.6$ Hz, 3H), 7.05–6.98 (m, 2H), 2.94 (t, $J = 7.6$ Hz, 4H), 2.12–1.93 (m, 16H), 1.71–1.64 (m, 4H), 1.49–1.40 (m, 4H), 1.38–1.25 (m, 8H), 1.17–0.95 (m, 48H), 0.93–0.84 (m, 6H), 0.81–0.52 (m, 40H); ^{13}C NMR (100 MHz, CDCl_3 , 25 °C, TMS): $\delta = 151.77, 151.56, 150.57, 150.38, 141.59, 141.39, 140.78, 140.39, 137.87, 137.70, 137.01, 136.32, 135.87, 135.71, 134.91, 132.01, 130.89, 130.61, 130.32, 130.13, 129.88, 129.50, 129.36, 129.26, 128.88, 128.54, 127.95, 127.71, 127.20, 126.96, 126.53, 125.81, 124.70, 123.34, 120.82, 119.73, 119.42, 114.07, 113.98, 100.46, 54.87, 54.77, 40.79, 33.56, 31.47, 31.39, 30.24, 29.76, 29.68, 29.14, 28.57, 28.43, 23.79, 22.57, 22.51, 22.43, 22.23, 14.02$. MS (MALDI-TOF, m/z): calcd for $\text{C}_{158}\text{H}_{188}\text{I}_2\text{S}_2$, $[\text{M}^+]$ 2405.1; found, 2405.6. Elemental analysis: calcd for $\text{C}_{158}\text{H}_{188}\text{I}_2\text{S}_2$: C 78.90, H 7.88; found: C 78.64, H 7.72.

3. Result and discussion

3.1. Synthesis

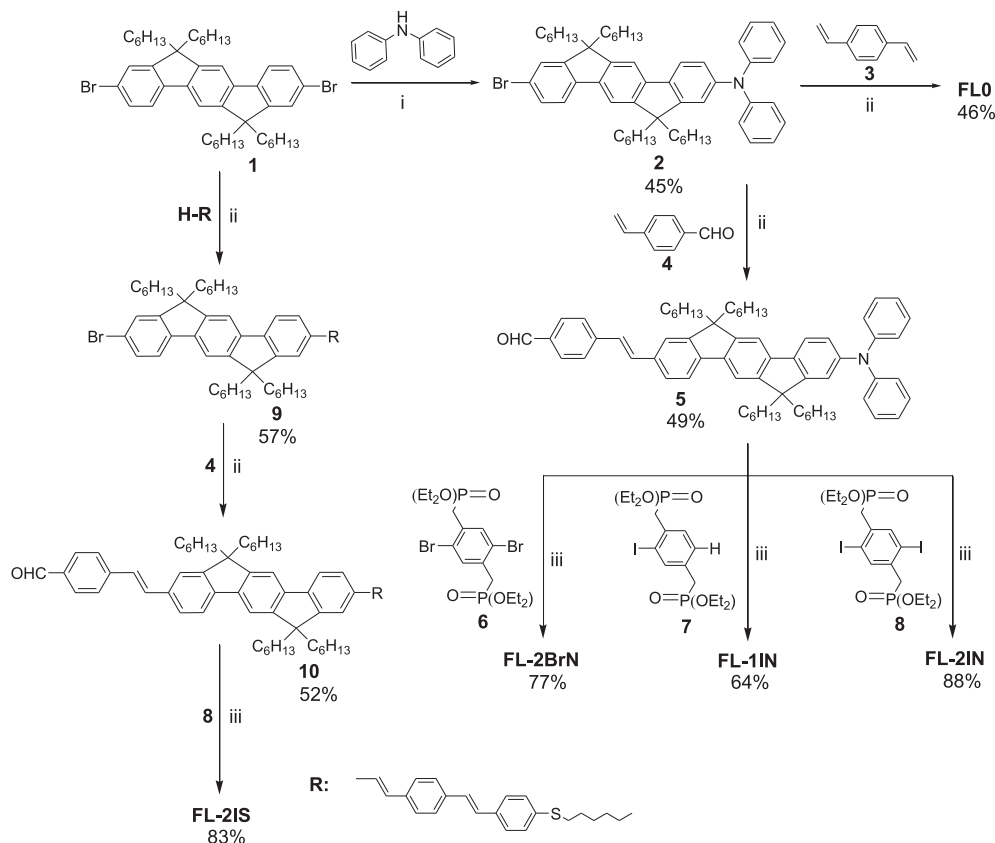
The synthetic routes for the two-photon photosensitizers are shown in Scheme 1. Compound **FLO** was prepared by a two-fold Heck reaction between the aryl bromide **2** and 1,4-

divinylbenzene **3** in 46% yield. Compounds **FL-2BrN**, **FL-11N**, **FL-2IN**, and **FL-2IS** were obtained in 64–88% yields by two-fold Horner–Emmons–Wittig coupling reactions of the phosphonates (**6**, **7**, or **8**) with an excess amount of the corresponding aldehydes (**5** and **10**) using sodium *tert*-butoxide as a base in THF at 0 °C. The intermediate aldehydes (**5** and **10**) were synthesized by reacting compounds **2** and **9** with 4-vinylbenzaldehyde (**4**) via Heck reactions in 49% and 52% yields, respectively. One-fold amination of compound **1** with diphenylamine afforded compound **2** in 45% yield. Compound **9** was obtained by a one-fold Heck reaction between compound **1** and (*E*)-hexyl(4-(4-vinylstyryl)phenyl)sulfane in 57% yield. All new compounds were characterized by ^1H NMR, ^{13}C NMR, MALDI-TOF MS, and the purity of the target chromophores were further confirmed by elemental analysis.

3.2. Linear absorption and emission

The linear absorption and emission spectra for compounds **FLO**, **FL-2IS**, **FL-11N**, **FL-2IN**, and **FL-2BrN** in THF are shown in Fig. 1, and the corresponding data are summarized in Table 1. As shown in Fig. 1, the linear absorption bands for these compounds were similarly located around 430 nm, and a bathochromic shift was observed in going from **FLO** (422 nm) to **FL-2IS** (423 nm), to **FL-11N** (424 nm), to **FL-2IN** (430 nm), and to **FL-2BrN** (434 nm). This trend in absorption for the chromophores is due to the negative inductive effect of the halogen atoms in the chromophore molecules and the extended π -conjugation length. For example, compound **FLO** with no halogen atom and a shorter π -conjugation length has an absorption maximum at 422 nm, while the absorption maximum of compound **FL-2IN** with two iodine atoms and a longer π -conjugation length shifts to 430 nm. Compound **FL-2BrN** has the same π -conjugation length as compound **FL-2IN**, whereas the former compound has a red-shifted absorption maximum of 434 nm, due to the stronger negative inductive effect of the bromine atom. On the other hand, the number of halogen atoms in the chromophore molecules also affects their absorption maxima. As an example, chromophore **FL-2IN** with two iodine atoms has a red-shifted absorption maximum compared to that of chromophore **FL-11N** with one iodine atom. For the emission spectrum of compound **FLO**, there were two emission peaks, at around 477 nm and 494 nm. However, only one emission peak was found for compounds **FL-2IS**, **FL-11N**, **FL-2IN**, and **FL-2BrN**. This difference may be due to the more nonpolar nature of compound **FLO** without halogen atoms, which may disturb the solvent-chromophore interactions. The emission maxima of the chromophores follow the same trend as that observed in their absorption maxima. As listed in Table 1, the emission peaks for the chromophores follow this order: **FLO** (472 nm) < **FL-2IS** (491 nm) < **FL-11N** (518 nm) < **FL-2IN** (543 nm) < **FL-2BrN** (552 nm). Similarly, the same trend was also found in the Stokes shifts of these chromophores, which follows the same order: **FLO** < **FL-2IS** < **FL-11N** < **FL-2IN** < **FL-2BrN**. For instance, compound **FLO** has a Stokes shift of 2510 cm^{-1} , whereas the Stokes shift value for compound **FL-2BrN** is 4925 cm^{-1} . This increased Stokes shift for the compound with a halogen atom can be attributed to its more polar nature which somewhat improves the solute/solvent interactions.

As shown in Table 1, the molar extinction coefficients of each compound in THF are relatively large with a range from $1.43 \times 10^5\text{ M}^{-1}\text{ cm}^{-1}$ to $2.52 \times 10^5\text{ M}^{-1}\text{ cm}^{-1}$, and the values follow this order: **FLO** > **FL-2BrN** > **FL-11N** > **FL-2IS** > **FL-2IN**. The molar extinction coefficient becomes smaller with the increasing size of the halogen atom. This is apparently associated with a decrease in the oscillator strength of the $S_0 \rightarrow S_1$ transition as a result of the substitution of the heavier atom [37]. Meanwhile, the fluorescence quantum yields (Φ_f) follow this order: **FLO** (0.53) > **FL-2BrN**



Scheme 1. Synthetic routes to chromophores **FLO**, **FL-2BrN**, **FL-1IN**, **FL-2IN**, and **FL-2IS**. (i) $\text{Pd}_2(\text{dba})_3$, dppf, *t*-BuONa, toluene, 100 °C; (ii) $\text{Pd}(\text{OAc})_2$, *P*(*o*-tolyl) $_3$, Et_3N , MeCN, reflux; (iii) *t*-BuONa, THF, 0–20 °C.

(0.37) > **FL-1IN** (0.27) > **FL-2IS** (0.25) > **FL-2IN** (0.22). These large changes in Φ_f are also attributed to a strong heavy atom effect. The decreased fluorescence quantum yields indicate an increase in the ISC rate, therefore, an increased generation of $^1\text{O}_2$ would be expected.

3.3. Two-photon absorption and emission

TPA spectra were determined by using laser pulses (<120 fs) tunable from 730 to 860 nm generated by a mode locked

Ti:sapphire laser. The data were obtained by a two-photon excited fluorescence method with fluorescein (80 μM in water, pH = 11) as a reference [38]. TPA cross-section (σ_2) peak values of these five chromophores in THF solution (2×10^{-6} M) were determined and listed in Table 2. Fig. 2 shows the TPA spectra of **FLO**, **FL-2IS**, **FL-1IN**, **FL-2IN**, and **FL-2BrN** with different halogen atoms. As shown in Fig. 2, these chromophores have TPA bands centered at around ~770 nm and the σ_2 peak values for compounds **FLO**, **FL-2IS**, **FL-1IN**, **FL-2IN**, and **FL-2BrN**, are 2084, 2319, 2471, 2564 and 2707 GM, in that order. In comparison with our previous reported ladder-type oligo-*p*-phenylene based chromophores [23], these new chromophores have larger TPA cross-section values, due to the extended π -conjugation lengths. Similarly, the σ_2 peak values of compounds with longer π -conjugation lengths (**FL-2IS**, **FL-1IN**, **FL-2IN**, and **FL-2BrN**) are larger than that of compound **FLO** with a shorter π -

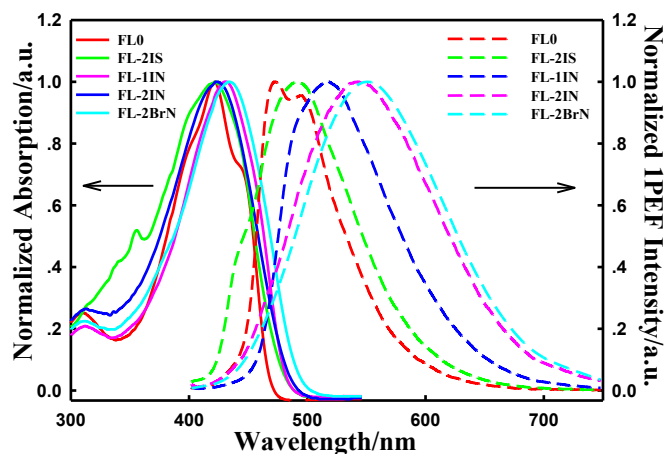


Fig. 1. Normalized absorption (solid lines) and fluorescence (dash lines) spectra of **FLO**, **FL-2IS**, **FL-1IN**, **FL-2IN**, and **FL-2BrN** in THF.

Table 1
Linear photophysical properties of compounds **FLO**, **FL-2IS**, **FL-1IN**, **FL-2IN**, and **FL-2BrN** in THF.

Compounds	λ_{abs} (nm) ^a	ϵ_{max} ($\text{M}^{-1} \text{cm}^{-1}$) ^b	λ_{em} (nm) ^c	$\Delta\nu$ (cm^{-1}) ^d	Φ_f ^e
FLO	422	2.52×10^5	472	2510	0.53
FL-2IS	423	1.76×10^5	491	3330	0.25
FL-1IN	424	1.84×10^5	518	4279	0.27
FL-2IN	430	1.43×10^5	543	4839	0.22
FL-2BrN	434	2.17×10^5	552	4925	0.37

^a Linear absorption peaks.

^b Molar extinction coefficient.

^c One-photon excited emission peaks.

^d Stokes shift.

^e Fluorescence quantum yields determined by using Fluorescein ($\Phi_f = 0.90$ in water, pH = 11) as the reference.

Table 2
Photophysical properties of compounds **FLO**, **FL-2IS**, **FL-1IN**, **FL-2IN**, and **FL-2BrN**.

Compounds	Maximum σ_2 (GM) ^a	σ'_2 (GM) ^b	Φ_Δ ^c
FLO	2084	1105	0.24
FL-2IS	2319	580	0.81
FL-1IN	2471	667	0.70
FL-2IN	2564	564	1.00
FL-2BrN	2707	1002	0.52

^a Maximum TPA cross section value by the fluorescence method in THF.

^b TPA action cross section $\sigma'_2 = \Phi_f \times \sigma_2$.

^c Relative $^1\text{O}_2$ yields that were normalized to that of **FL-2IN**.

conjugation length. It can be found that besides the effect of the π -conjugation length on the σ_2 value, the substituted halogen atoms (such as Br, I) at the phenyl ring of the core also affect the maximal σ_2 values. For example, the σ_2 peak value of compound **FL-1IN** is 2319 GM, while with the same π -conjugation length, compound **FL-2BrN** has a σ_2 peak value of 2707 GM. This difference can be due to the introduction of the electron withdrawing halogen atoms in the core, creating a donor-acceptor-donor (D-A-D) motif, leading to the increased extent of charge transfer from the ends of the molecule to the center, namely an increased intramolecular charge transfer (ICT). As it has been known that large TPA is associated with the extent of ICT for a given molecule. Obviously, compound **FL-2BrN** has a stronger ICT, because of the stronger electron withdrawing ability of bromine compared to that of iodine. Notably, although compound **FL-2IS** has a longer π -conjugation length, its σ_2 value is smaller than those of compounds **FL-1IN** and **FL-2IN**, which can be also attributed to the enhancement of ICT by incorporating the strong electron donating diarylamino groups into **FL-1IN** and **FL-2IN**. The result is also consistent with our previous studies [24].

Two-photon excited fluorescence (TPEF) spectra of the two-photon absorbing chromophores **FLO**, **FL-2IS**, **FL-1IN**, **FL-2IN**, and **FL-2BrN** were recorded in THF solution (2×10^{-6} M) at room temperature by using an Ocean Optics s2000 spectrometer in conjunction with a fiber coupler head (Fig. 3). Under these conditions, the intensity for two-photon excitation was in an excitation regime where the fluorescence signal showed a quadratic dependence on the intensity of the excitation beam, as expected for two-photon induced emission. As an example, the log–log plots show slopes of 2.02 and 1.96 for compounds **FLO** and **FL-2IN**, respectively (inset of Fig. 3).

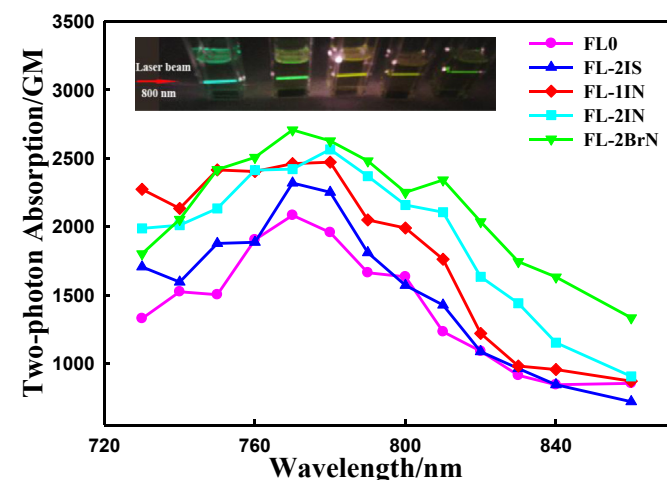


Fig. 2. TPA spectra for the indenofluorene-based chromophores in THF measured by the two-photon excited fluorescence method.

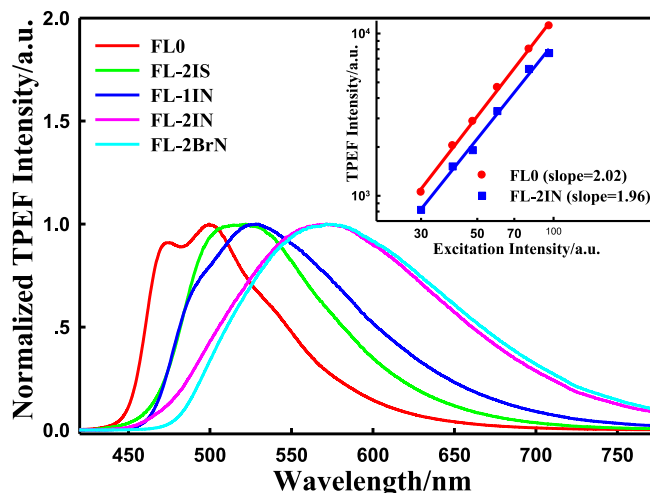


Fig. 3. Two-photon excited fluorescence (TPEF) spectra for the indenofluorene-based chromophores in THF and their peak intensity versus the laser intensity at 800 nm (inset).

As shown in Fig. 3, upon an excitation by 800 nm laser pulses, all the chromophores emitted frequency-upconverted fluorescence with emission maxima (λ_{max}) in the range of 498–573 nm. For example, the two-photon excited emission peaks of **FLO**, **FL-2IS**, **FL-1IN**, **FL-2IN**, and **FL-2BrN** in THF were 498, 516, 527, 568, and 573 nm, in that order. Similar to their linear emission in THF, compound **FL-2BrN** has a red-shifted emission band compared to that for compound **FLO**. From Figs. 1 and 3, one may find that the TPE fluorescence spectra for compounds **FLO**, **FL-2IS**, **FL-1IN**, **FL-2IN**, and **FL-2BrN** in THF are basically the same as their linear fluorescence spectra, which confirms that both emissions are from the same excited state, although different excitation processes and different selection rules are applied for TPEF and one-photon excited fluorescence.

For the application of two-photon materials in fluorescence imaging, it is important to know the TPA action cross section σ'_2 ($\sigma'_2 = \sigma_2 \times \Phi_f$), where σ_2 is the TPA cross section and Φ_f is the fluorescence quantum yield, on condition that the Φ_f values for both one- and two-photon excited fluorescence are the same. As listed in Table 2, all the five chromophores have much larger TPA action cross section values compared to most of commercial dyes. The σ'_2 values of **FLO** and **FL-2BrN** (1105 and 1002 GM) are larger than those of the others. **FL-2IS**, **FL-1IN** and **FL-2IN** show relatively low σ'_2 values of 580, 667, and 564 GM due to their relatively low Φ_f values although they have large σ_2 values. The two-photon excited fluorescence of these chromophores can be directly observed with naked eyes (inset of Fig. 2) due to their high active TPA action cross sections. It can be expected that these new chromophores are good candidates for two-photon imaging applications.

3.4. Quantum yield of $^1\text{O}_2$ generation (Φ_Δ)

Φ_Δ is a very important measure of the efficiency of photosensitization. A high $^1\text{O}_2$ generation efficiency is required for the PDT application of photosensitizers. $^1\text{O}_2$ generation efficiencies of compounds **FLO**, **FL-2BrN**, **FL-1IN**, **FL-2IS**, and **FL-2IN** in air-saturated toluene solution were evaluated by monitoring the characteristic emission peak of singlet oxygen at ~1270 nm at room temperature using 9,10-dibromoanthracene (**DBA**) as a reference ($\Phi_\Delta = 0.85$) [39,40]. The concentrations of all solutions were adjusted to give an optical density (OD) of 0.5 at 430 nm. Then, the

$^1\text{O}_2$ generation yield (Φ_Δ) of a sample under one-photon excitation can be calculated according to the following equation:

$$\phi_\Delta^s = \phi_\Delta^r \cdot \frac{I_s \cdot A_r \cdot \tau_r}{I_r \cdot A_s \cdot \tau_s} \quad (1)$$

Where I is the emission intensity of singlet oxygen at ~ 1270 nm, A is the absorbance of the solution, τ is the lifetime of singlet oxygen phosphorescence in the selected solvent [41].

Under an excitation at 430 nm, five compounds all displayed the characteristic $^1\text{O}_2$ emission band at ~ 1270 nm (Fig. 4), which confirms that the $^1\text{O}_2$ generated from the interaction between the photosensitizers and the molecular oxygen. The luminescence intensities for chromophores **FLO**, **FL-2BrN**, **FL-11N**, **FL-2IS**, **FL-2IN** and **DBA** follow this order: 463, 1006, 1341, 1574, 1898, and 2305. Obviously, the $^1\text{O}_2$ luminescence intensity of **FL-2IN** is significantly stronger than those of the other photosensitizers with the same OD, which indicates that **FL-2IN** has a higher $^1\text{O}_2$ generation efficiency. According to Equation (1), the Φ_Δ values of **FLO**, **FL-2BrN**, **FL-11N**, **FL-2IS**, and **FL-2IN** were 0.17, 0.37, 0.49, 0.58 and 0.70, in that order (Table 2). The Φ_Δ values become larger with the increasing size of the halogen atom. Compared with **FLO**, the $^1\text{O}_2$ generation yields of **FL-2BrN**, to **FL-11N**, to **FL-2IS**, and to **FL-2IN**, are enhanced by factors of 2.2, 2.9, 3.4, and 4.1, in that order. The enhanced generation of $^1\text{O}_2$ for the molecules with halogen atoms (Br, or I) incorporated is attributed to the increase of ISC rate induced by the heavy atom effect. Correspondingly, decreased fluorescence quantum yields were found for the molecules with halogen atoms in agreement with their increased ISC rates.

Two-photon induced $^1\text{O}_2$ generation of the chromophores in air-saturated toluene was also evaluated by a chemical trapping method using 1,3-diphenylisobenzofuran (**DPBF**), a well-known singlet oxygen indicator [42]. In this method, **DPBF** reacts with $^1\text{O}_2$ to form peroxide, which leads to a decrease in the absorption of **DPBF** at 418 nm. The UV absorption at 418 nm was monitored during the course of irradiation by a laser beam at 808 nm in the presence of photosensitizers. The blank control experiments were performed in the presence of only **DPBF** at the same conditions. The curve of decrease in the absorption at 418 nm of **DPBF** was plotted as a function of the irradiation time. As shown in Fig. 5, throughout the irradiation time, no obvious changes of the absorption intensity of **DPBF** were observed for the blank sample. However, significant decreases of the absorption intensity of **DPBF** at 418 nm in the

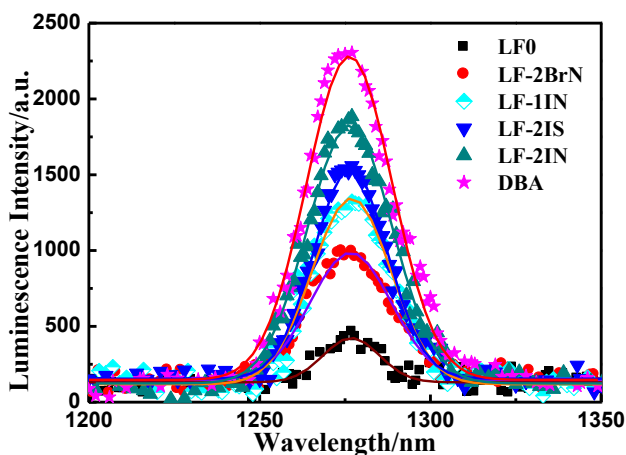


Fig. 4. Luminescence of $^1\text{O}_2$ sensitized with the indenofluorene-based chromophores, and **DBA**, with an excitation at 430 nm in toluene solutions. Gaussian fits are shown for every emission curve (solid line).

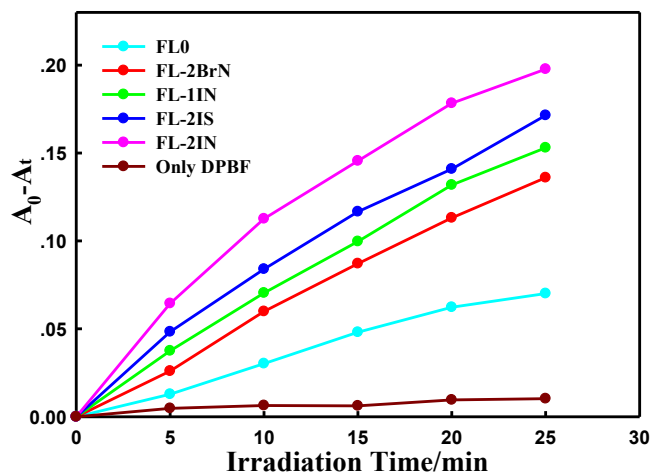


Fig. 5. Plots of change in the absorbance of **DPBF** at 418 nm versus interval irradiation time in the presence of the indenofluorene-based chromophores in air-saturated toluene solution under a laser irradiation at 808 nm. A_0 is the initial absorption, A_t is the absorption after irradiating for an interval of time.

presence of the five photosensitizers were observed and the photo-oxidation rates of **DPBF** for these compounds were in this order: **FLO** < **FL-2BrN** < **FL-11N** < **FL-2IS** < **FL-2IN**. The results are in agreement with their $^1\text{O}_2$ generation capability induced by one-photon excitation. Similarly, the photo-oxidation rate of **DPBF** in the presence of **FL-2IN** is obviously faster than those of the others under two-photon excitation, also indicating that **FL-2IN** has a higher $^1\text{O}_2$ generation capability and can act as a better photosensitizer for two-photon PDT.

3.5. Cytotoxicity against cancer cells

Good biocompatibility and low dark cytotoxicity are essential for photosensitizers in biological applications. To evaluate **FL-2IN** as an effective photosensitizer for two-photon PDT of tumors, the in vitro cytotoxicity against MCF-7 (human breast adenocarcinoma cell line) cells was investigated by a MTT assay. The toxicities of **FL-2IN** at varying concentrations were tested in the dark or under a laser beam irradiation. As seen from Fig. 6a, after incubation for 24 h in dark, **FL-2IN** showed no obvious cytotoxicity effect on MCF-7 cells in the concentrations range from 5 to 10 μM . However, the dark cytotoxicity increased with the increasing concentration of compound **FL-2IN**. For example, when the concentration of compound **FL-2IN** increased from 5 μM , to 10 μM , 20 μM , and 40 μM , the viabilities of cells decreased from 96.4%, to 92.3%, 86.2%, and 78.2%, respectively. The photo-toxicity of **FL-2IN** was conducted using a laser at 808 nm with a light intensity of $\sim 3.0 \text{ W cm}^{-2}$. The laser beam was unfocused, and has a beam size of $\sim 4.0 \text{ cm}^2$. The irradiation time was 10, 20, or 40 min, giving a light dose of 1800 J cm^{-2} , 3600 J cm^{-2} , and 7200 J cm^{-2} , respectively. The plate without compound **FL-2IN** was used as a control. As shown in Fig. 6b, laser irradiation alone caused almost no cytotoxicity (<2% cell death) at all in the absence of **FL-2IN**. In contrast, in the presence of compound **FL-2IN** in concentration range from 0 to 40 μM , the viabilities of cells decreased progressively with the increasing laser irradiation time. For example, at the concentration of 40 μM , the viabilities of cells are 71.5%, 56.7%, and 48.3% after irradiation for 10, 20, and 40 min, respectively. Meanwhile, under the same irradiation time, increased cell death was found with the increasing amount of drug loaded. For example, after an irradiation of 40 min, the viabilities of cells are 84.8%, 76.6%, 64.2%, and 48.3% with increasing concentration of

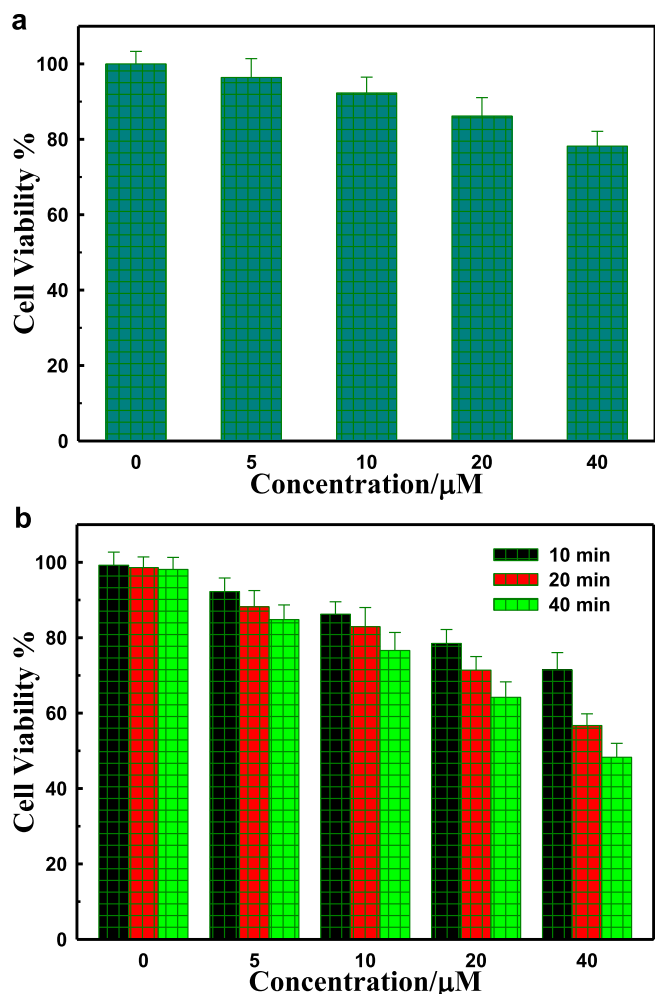


Fig. 6. (a) The dark cytotoxicity of **FL-2IN** at different concentrations towards MCF-7 cells. (b) Photo-toxicity of **FL-2IN** at different concentrations towards MCF-7 cells after the 808 nm laser irradiation with different irradiation times. The control experiment without any photosensitizers was performed under the same experimental conditions.

FL-2IN from 5 to 40 μM . Notably, increased concentration of compound **FL-2IN** also leads to its increased dark cytotoxicity. Considering the dark cytotoxicity induced by compound **FL-2IN**, one may still observe an increase of cell death induced by the increased $^1\text{O}_2$ generation. For example, after an irradiation for 40 min, the death rate of MCF-7 cells increases from 11.6% to 29.9%, when the concentration of compound **FL-2IN** increases from 5 to 40 μM . These preliminary results indicate the feasibility of employing two-photon photosensitizer for PDT and **FL-2IN** can act as an efficient photosensitizer for two-photon photodynamic treatment on cancer cells. It should be noted that **FL-2IN** can be dispersed in water to form nanoparticles using a reprecipitation method with the aid of DMSO, and the size of the resulting nanoparticles is about 10 nm. (Fig. 7) [43]. The linear absorption and emission spectra for the **FL-2IN** nanoparticles in aqueous solution are basically the same as those of **FL-2IN** in THF except for slightly red-shifted absorption and emission bands for the latter. However, the fluorescence quantum yield for **FL-2IN** in aqueous solution decreases to 0.17 due to a stronger solvent-solute interaction in the high polar environment (H_2O). Further, the biocompatibility of these type photosensitizers can be further improved through the incorporation of polar group into the photosensitizer structures, which may also reduce their dark cytotoxicity.

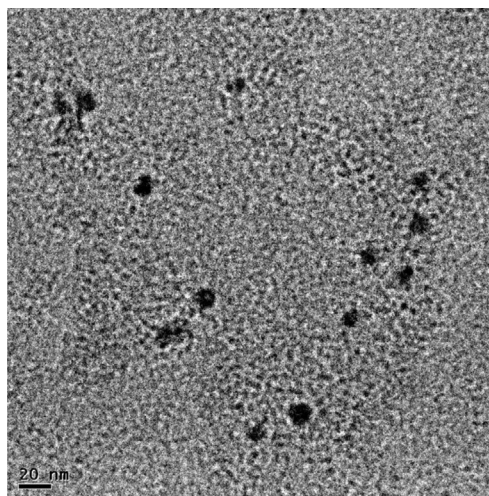


Fig. 7. The TEM image of **FL-2IN** nanoparticles obtained by the reprecipitation method.

4. Conclusions

A series of indenofluorene-based chromophores have been designed and synthesized as two-photon active photosensitizers for PDT. Heavy atoms (Br, I) were incorporated into the backbone of the indenofluorene-based chromophores to enhance their singlet oxygen generation efficiencies. The TPA spectra for these chromophores were determined by using the two-photon excited fluorescence method. With the incorporated heavy atoms, chromophores **FL-2IS**, **FL-1IN**, **FL-2IN**, and **FL-2BrN** exhibited larger TPA cross section peak values compared to the chromophore (**FLO**) without a heavy atom. The singlet oxygen generation efficiencies of these photosensitizers under one- and two-photon excitation have also been evaluated. **FL-2IN** showed a 410% higher Φ_{Δ} value in comparison with **FLO**, due to the strong heavy atom effect. Moreover, the high TPA cross-section value of **FL-2IN** in combination with its high Φ_{Δ} value makes it a promising photosensitizer for two-photon PDT. **FL-2IN** provided a moderate two-photon PDT efficacy against cancer cells. These results suggest that the introduction of heavy atoms into two-photon absorbing chromophores can be an efficient strategy to enhance the two-photon excited singlet oxygen generation efficiencies of photosensitizers. Future work will focus on covalently coupling the two-photon photosensitizers with targeting biomolecules to improve their biocompatibility and selectivity towards cancer cells in PDT.

Acknowledgments

This work was in part supported by the Natural Science Foundation of China (Nos 21102144 61325026, and 11104266), in part supported by 100 Talents Programme of the Chinese Academy of Sciences, in part supported by Special Project of National Major Scientific Equipment Development of China (2012YQ120060) and The CAS/SAFEA International Partnership Program for Creative Research Teams.

References

- [1] Lovell JF, Liu TWB, Chen J, Zheng G. Activatable photosensitizers for imaging and therapy. *Chem Rev* 2010;110:2839–57.
- [2] Kamkaew A, Lim SH, Lee HB, Kiew LV, Chung LY, Burgess K. Bodipy dyes in photodynamic therapy. *Chem Soc Rev* 2013;42:77–88.
- [3] Dolmans DE, Fukumara D, Jain RK. Photodynamic therapy for cancer. *Nat Rev Cancer* 2003;3:380–7.

- [4] Ogilby PR. Singlet oxygen: there is indeed something new under the sun. *Chem Soc Rev* 2010;39:3181–209.
- [5] Lu T, Shao P, Mathew I, Sand A, Sun W. Synthesis and photophysics of benzotexaphyrin: a near-infrared emitter and photosensitizer. *J Am Chem Soc* 2008;130:15782–3.
- [6] Xia Q, Boudreau MD, Zhou Y-T, Yin J-J, Fu PP. Uvb photoirradiation of aloe vera-formation of free radicals, singlet oxygen, superoxide, and induction of lipid peroxidation. *J Food Drug Anal* 2011;19:396–402.
- [7] Cadet J, Ravanat J-L, Martinez GR, Medeiros MHG, Mascio PD. Singlet oxygen oxidation of isolated and cellular DNA: product formation and mechanistic insights. *Photochem Photobiol* 2006;82:1219–25.
- [8] Tørring T, Helmig S, Ogilby PR, Gothelf KV. Singlet oxygen in DNA nanotechnology. *Acc Chem Res* 2014;47:1799–806.
- [9] Davies MJ. Singlet oxygen-mediated damage to proteins and its consequences. *Biochem Biophys Res Commun* 2003;305:761–70.
- [10] Jensen RL, Arnbjerg J, Ogilby PR. Reaction of singlet oxygen with tryptophan in proteins: a pronounced effect of the local environment on the reaction rate. *J Am Chem Soc* 2012;134:9820–6.
- [11] Celli JP, Spring BQ, Rizvi I, Evans CL, Samkoe KS, Verma S, et al. Imaging and photodynamic therapy: mechanisms, monitoring, and optimization. *Chem Rev* 2010;110:2795–838.
- [12] Pawlicki M, Collins HA, Denning RG, Anderson HL. Two-photon absorption and the design of two-photon dyes. *Angew Chem Int Ed* 2009;48:3244–66.
- [13] Ogawa K, Kobuke Y. Recent advances in two-photon photodynamic therapy. *AntiCancer Agents Med Chem* 2008;8:269–79.
- [14] Oar MA, Serin JM, Dichtel WR, Fréchet JM, Ohulchanskyy TY, Prasad PN. Photosensitization of singlet oxygen via two-photon-excited fluorescence resonance energy transfer in a water-soluble dendrimer. *Chem Mater* 2005;17:2267–75.
- [15] Tian Y, Chen CY, Cheng YJ, Young AC, Tucker NM, Jen AY. Hydrophobic chromophores in aqueous micellar solution showing large two-photon absorption cross sections. *Adv Funct Mater* 2007;17:1691–7.
- [16] Chen C-Y, Tian Y, Cheng Y-J, Young AC, Ka J-W, Jen AK-Y. Two-photon absorbing block copolymer as a nanocarrier for porphyrin: energy transfer and singlet oxygen generation in micellar aqueous solution. *J Am Chem Soc* 2007;129:7220–1.
- [17] Shen X, Li L, Min Chan AC, Gao N, Yao SQ, Xu Q-H. Water-soluble conjugated polymers for simultaneous two-photon cell imaging and two-photon photodynamic therapy. *Adv Opt Mater* 2013;1:92–9.
- [18] Beverina L, Crippa M, Landenna M, Ruffo R, Salice P, Silvestri F, et al. Assessment of water-soluble π -extended squaraines as one- and two-photon singlet oxygen photosensitizers: design, synthesis, and characterization. *J Am Chem Soc* 2008;130:1894–902.
- [19] Pimenta FM, Jensen RL, Holmegaard L, Esipova TV, Westberg M, Breitenbach T, et al. Singlet-oxygen-mediated cell death using spatially-localized two-photon excitation of an extracellular sensitizer. *J Phys Chem B* 2012;116:10234–46.
- [20] Zou Q, Fang Y, Zhao Y, Zhao H, Wang Y, Gu Y, et al. Synthesis and in vitro photocytotoxicity of coumarin derivatives for one- and two-photon excited photodynamic therapy. *J Med Chem* 2013;56:5288–94.
- [21] He GS, Tan L-S, Zheng Q, Prasad PN. Multiphoton absorbing materials: molecular designs, characterizations, and applications. *Chem Rev* 2008;108:1245–330.
- [22] Lin T-C, Li M-L, Liu C-Y, Tsai M-Y, Lee Y-H, Febriani Y, et al. Synthesis and two-photon properties of multi-branched fluorophores composed of ladder-type conjugated cores and functionalized diquinoxalinyllamino peripheries. *Eur J Org Chem* 2014;2014:1615–21.
- [23] Zheng Q, Gupta SK, He GS, Tan LS, Prasad PN. Synthesis, characterization, two-photon absorption, and optical limiting properties of ladder-type oligo-*p*-phenylene-cored chromophores. *Adv Funct Mater* 2008;18:2770–9.
- [24] Tang C, Zheng Q, Zhu H, Wang L, Chen S-C, Ma E, et al. Two-photon absorption and optical power limiting properties of ladder-type tetraphenylene cored chromophores with different terminal groups. *J Mater Chem C* 2013;1:1771–80.
- [25] Gorman A, Killoran J, O'Shea C, Kenna T, Gallagher WM, O'Shea DF. In vitro demonstration of the heavy-atom effect for photodynamic therapy. *J Am Chem Soc* 2004;126:10619–31.
- [26] Kim S, Ohulchanskyy TY, Bharali D, Chen Y, Pandey RK, Prasad PN. Organically modified silica nanoparticles with intraparticle heavy-atom effect on the encapsulated photosensitizer for enhanced efficacy of photodynamic therapy. *J Phys Chem C* 2009;113:12641–4.
- [27] Yogo T, Urano Y, Ishitsuka Y, Maniwa F, Nagano T. Highly efficient and photostable photosensitizer based on bodipy chromophore. *J Am Chem Soc* 2005;127:12162–3.
- [28] Zheng Q, He GS, Lu C, Prasad PN. Synthesis, two- and three-photon absorption, and optical limiting properties of fluorene-containing ferrocene derivatives. *J Mater Chem* 2005;15:3488–93.
- [29] Zhang K, Dai Y, Zhang X, Xiao Y. Synthesis and photophysical properties of three ladder-type chromophores with large and rigid conjugation structures. *Dyes Pigments* 2014;102:1–5.
- [30] Fan HH, Guo L, Li KF, Wong MS, Cheah KW. Exceptionally strong multiphoton-excited blue photoluminescence and lasing from ladder-type oligo(*p*-phenylene)s. *J Am Chem Soc* 2012;134:7297–300.
- [31] Bigot YL, Delmas M, Gaset A. A simplified wittig synthesis using solid/liquid transfer processes IV – synthesis of symmetrical and asymmetrical mono- and di-olefins from terephthalic aldehyde. *Synth Commun* 1983;13:177–82.
- [32] Bonifacio MC, Robertson CR, Jung J-Y, King BT. Polycyclic aromatic hydrocarbons by ring-closing metathesis. *J Org Chem* 2005;70:8522–6.
- [33] Sy W-W, Lodge BA, By AW. Aromatic iodination with iodine and silver sulfate. *Synth Commun* 1990;20:877–80.
- [34] Vaidyanathan G, Shankar S, Affleck DJ, Alston K, Norman J, Welsh P, et al. Meta-iodobenzylguanidine derivatives containing a second guanidine moiety. *Bioorg Med Chem* 2004;12:1649–56.
- [35] Gaefke G, Enkelmann V, Höger S. A practical synthesis of 1,4-diiodo-2,5-bis(chloromethyl)benzene and 1,4-diiodo-2,5-bis(bromomethyl)benzene. *Synthesis* 2006;2006:2971–3.
- [36] Wilson JN, Windscheif PM, Evans U, Myrick ML, Bunz UH. Band gap engineering of poly(*p*-phenyleneethynylene)s: cross-conjugated ppe-ppv hybrids. *Macromolecules* 2002;35:8681–3.
- [37] Nijegorodov N, Mabbs R. The influence of molecular symmetry and topological factors on the internal heavy atom effect in aromatic and heteroaromatic compounds. *Spectrochim Acta Part A* 2001;57:1449–62.
- [38] Xu C, Webb WW. Measurement of two-photon excitation cross sections of molecular fluorophores with data from 690 to 1050 nm. *J Opt Soc Am B* 1996;13:481–91.
- [39] Brauer H-D, Acs A, Drews W, Gabriel R, Ghaeni S, Schmidt R. Generation of $^1\text{O}_2$ from oxygen quenching of the lowest excited singlet and triplet states of some aromatic compounds. *J Photochem* 1984;25:475–88.
- [40] Nosaka Y, Daimon T, Nosaka AY, Murakami Y. Singlet oxygen formation in photocatalytic TiO_2 aqueous suspension. *Phys Chem Chem Phys* 2004;6:2917–8.
- [41] Tanielian C, Heinrich G. Effect of aggregation on the hematoporphyrin-sensitized production of singlet molecular oxygen. *Photochem Photobiol* 1995;61:131–5.
- [42] Mirenda MN, Strassert CA, Dicalio LE, Roman ES. Dye-polyelectrolyte layer-by-layer self-assembled materials: molecular aggregation, structural stability, and singlet oxygen photogeneration. *ACS Appl Mater Inter* 2010;2:1556–60.
- [43] Baba K, Pudavar HE, Roy I, Ohulchanskyy TY, Chen Y, Pandey RK, et al. New method for delivering a hydrophobic drug for photodynamic therapy using pure nanocrystal form of the drug. *Mol Pharmacol* 2007;4:289–97.